*Desalination and Water Treatment*
www.deswater.com

doi: 10.5004/dwt.2019.24075

155 (2019) 381–389
July

# Poly (vinyl chloride)-MMT composite membranes with enhanced properties and separation performance

Adel A. El-Zahhar, Majed M. Alghamdi*, Badriah M. Asiri

*Department of Chemistry, Faculty of Science, King Khalid University, P.O. Box 9004, Abha 61413, Saudi Arabia, emails: mmalghamdi@kku.edu.sa (M.M. Alghamdi), elzahhar@kku.edu.sa (A.A. El-Zahhar), bdra3h2@hotmail.com (B.M. Asiri)*

Received 27 September 2018; Accepted 3 March 2019

**ABSTRACT**

In this paper, we report on the characterization and performance of reasonably low-cost composite membranes of poly (vinyl chloride) (PVC) and montmorillonite (MMT) clay. Composite membranes were fabricated using different MMT loading levels (0–10 wt%), using a phase-inversion method to improve the PVC membrane's physicochemical properties and performance. Membranes were characterized by X-ray diffraction, thermal gravimetric analysis, scanning electron microscopy, Fourier transform infrared spectroscopy, and contact angle measurements. X-ray diffraction studies revealed the formation of the MMT exfoliated structure. Thermal gravimetric analysis indicated improved thermal stability with the addition of MMT. Moreover, the experimental performance results demonstrated an improvement regarding water flux, antifouling properties, and salt rejection up to a loading of 10%. The membrane containing 6% MMT exhibited optimum performance, with 127% enhancement in water flux. Moreover, it demonstrated an improvement of 32% in the salt rejection for NaCl, $Na_2SO_4$ and $MgSO_4$ and 36% for LiCl, compared with the pure PVC membrane. Furthermore, it displayed an increase of 28% in the flux recovery ratio.

*Keywords:* Poly (vinyl chloride) (PVC); Membrane; Montmorillonite (MMT); Composite; Antifouling

## 1. Introduction

Although, membrane technology has rapidly developed, with membranes offering a wide range of advantages and new materials allowing for the creation of advanced membranes, poor performance and high costs have hindered their widespread use. The most commonly used polymers to prepare membranes include cellulose acetate (CA), polypropylene (PP), polysulfone (PS), polyacrylonitrile (PAN), polyvinylidene (PVDF), and polyethersulfone (PES) as well as inorganic membranes [1–6]. With regard to cost, inorganic membranes applications are usually limited because of their expensive materials and fabrication procedures. On the other hand, although polymer-based materials are reasonably cheaper, polymer backbones are highly hydrophobic and susceptible to extensive fouling; therefore, they cannot be used without modifications [7].

Several methods have been employed to enhance the performance of polymeric-based membranes by decreasing the fouling tendency and increasing hydrophilicity. These methods include surface coating [8], surface grafting [9,10], and blending with amphiphilic materials. However, surface grafting and coating are expensive and unlikely capable of large-scaling industrial manufacture, whereas blending amphiphilic has the potential for industrial production.

As physical blending is a reasonably straightforward method, it has been broadly applied to incorporate nanoparticles into membranes. Recently, this has attracted considerable attention. This is because the nanocomposite membranes have the capability to produce unique characteristics that can improve properties such as permeability, selectivity, chemical stability, and the operating pressure and temperature; they can also reduce the fouling tendency. Different types of nanomaterials, such as titanium oxide

* Corresponding author.

[11,12], zinc oxide [13,14], alumina [15], silica [16], graphene oxide [17], and carbon nanotubes [18,19], have been exploited with the aim of improving antifouling, solutes rejection, and water flux properties of fabricated membranes. For example, the employment of different types and sizes of $TiO_2$ nanoparticles into the membranes resulted in an improvment in properties such as hydrophilicity and antifouling, in addition to the improved thermal stability, mechanical strength, and higher water flux of the membranes [20–22]. Moreover, the incorporation of ZnO [13] and $Al_2O_3$ [15] into a membrane led to an observed improvement in membrane porosity and antifouling properties. Furthermore, higher water flux, flux recovery and hydrophilicity were reported with the addition of $SiO_2$ [23].

Nevertheless, poly (vinyl chloride) (PVC) composite membranes in particular have not attracted much attention. Although, PVC is one the most important commercial plastics due to its numerous applications and low cost, it still possesses many problems that need to be overcome in order to be used as a membrane. Still, as PVC can be dissolved in a variety of industrial solvents such as N-methyl-pyrrolidinone [14], N,N dimethylacetamide [24], tetrahydrofuran [25], and dimethylformamide [26], PVC may become a good candidate for industrial applications. However, the effect of various additives to the PVC membrane has not been sufficiently investigated and only a few studies have been reported in the leterature. For example, the effect of a polymeric additive (Pluronic F127) on the performance of the PVC membrane resulted in a reduction in the water permeability of the membranes due to the reduction in pore density and size [27]. Nevertheless, remarkable improvement in the antifouling properties of the membranes was reported. Moreover, lower mechanical properties and rejection was also observed as a result of PVP/PEG addition [28]. On the other hand, an enhancement of the hydrophilicity of the PVC membrane was reported by Peng et al. [29] by the addition of poly (vinyl butyral) along with higher permeation flux. Furthermore, the addition of nano-$Fe_2O_3$ was also found to lead to an improvement in properties and separation performance [30].

In addition to the employment of nanomaterials and other polymers as additives, polymer-clay composites are an example of the latest developed in inorganic-organic polymer reinforcement techniques. Although, the addition of MMT has demonstrated to improved mechanical properties, thermal stability [31–33], the performance of PVC-MMT composite as a membrane has not been investigated comprehensively. In the present work, PVC composite membranes with different loadings of MMT were prepared. The objective is to examine the influence of MMT on the characteristics and performance of the composite membranes, which may provide a novel technique for producing high performance and low-cost membranes.

## 2. Experimental setup

### 2.1. Materials

All chemicals used in the current study were analytical grades purchased from Sigma-Aldrich© (Germany) and were used as received.

### 2.2. Membrane preparation

Membrane composites of PVC-MMT were prepared via the phase-inversion technique. First, different amounts of MMT were dispersed in dimethylformamide (DMF) and stirred for one hour to verify complete dispersion of MMT particles in the solvent. The obtained suspension was then sonicated for one hour to make sure that particles were well dispersed in the solution. Second, the PVC, with 17 wt% in DMF, was prepared and stirred until completely dissolved. After that, the prepared MMT suspension was added to the PVC solution with continuous stirring for 12 h until a homogenous solution was formed. Absolute compositions of the prepared casting solutions are shown in Table 1. Next, to remove air bubbles, a vacuum oven was used for 12 h before the solution was casted on a glass plate. A casting knife with a thickness of 0.6 mm was then utilized to obtain the casted film; this was immediately submerged into a coagulation bath of distilled water. After that, obtained film was washed several times with distilled water to remove the residual solvent, and then stored in distilled water for further examination.

## 3. Membrane characterization

Fourier transform infrared (FT-IR) analysis was performed using Nicolet 6700 FT-IR from Thermo Scientific, where the samples were mixed with potassium bromide and compressed to obtain a disk. The spectra of the obtained disks were analyzed in the IR region of 4,000–400 $cm^{-1}$. A Shimadzu 6000DX (from the Shimadzu Corporation, Japan) was used to carry out the XRD analysis, using the following operating conditions: CuK$\alpha$ sealed tube operated at 40 kV and 30mA, measured from 5 to 80° 2$\theta$ at 0.020 step with $\lambda$ = 0.154056 nm. All samples were analyzed in triplicate to obtain representative results and the average was considered. Other instrumental parameters were appropriately fitted for samples. Moreover, field emission scanning electron microscopy was used for the evaluation of the morphology of the samples. Images were obtained using a Jeol Model 6360 LV SEM (USA). Furthermore, thermal gravimetric analysis was measured (25°C–800°C) on Shimadzu TGA-50H thermal analyzers. The sample with 15 mg was heated in platinum crucible within a temperature range of 30°C–800°C, with a heating rate of 10°C $min^{-1}$ with a controlled nitrogen flow of 40 $cm^3$ $min^{-1}$. Also, the static water contact angle was used to evaluate the hydrophilicity and wetability of the membrane surface using distilled water.

## 4. Membrane properties

Properties that included porosity, water uptake, and pore size analysis were investigated. The volume fraction method

Table 1
Casting solutions composition for PVC, PVC-MMT %

| Membrane code | PVC (wt/wt%) | MMT (wt/wt%) |
|---|---|---|
| PVC | 100 | 0 |
| PVC-MMT 2% | 98 | 2 |
| PVC-MMT 6% | 94 | 6 |
| PVC-MMT 10% | 90 | 10 |

was employed to calculate the porosity and water uptake values of the prepared membrane. The following equations were used for porosity and water uptake, respectively [13,34].

$$\varepsilon = \frac{W_{w-}W_d}{\rho_w\left(\pi r^2 l\right)} \times 100 \quad (1)$$

$$\text{Water uptake} = \frac{W_{w-}W_d}{W_d} \times 100 \quad (2)$$

where $W_w$ (g) denotes weight for a wet membrane, and $W_d$ (g) denotes the weight for a dry membrane. $l$ and $r$ (cm) are the thickness and radius of the membrane, respectively. $\rho_w$ (g 1cm$^3$)$^{-1}$ is the density of the water at 25°C.

The mean pore diameter of the prepared membrane was estimated according to the following equation [18, 20]:

$$a = \sqrt{\frac{\left(2.9 - 1.75\varepsilon\right) \times 8\mu l Q_w}{\varepsilon A \Delta P}} \quad (3)$$

where $a$ (m) is the mean pore diameter and $Q_w$ (m$^3$ s)$^{-1}$ is the pure water flux. $A$(m$^2$) and $l$ (m) are the filtration area of the membrane and the thickness of the membrane, respectively. μ (Pa.s) is the viscosity of the water at 25°C. $\Delta P$ (Pa) is the transmembrane pressure and ε is the porosity.

## 5. Membrane performance

### 5.1. Pure water flux and rejection ratio measurements

The performance of the membrane was studied using the dead-end membrane filtration system. The performance was likewise evaluated at different applied membrane pressures (0.2– 0.9 MPa) to monitor the membranes deformation with pressure. The applied membrane pressure (AMP) was manually adjusted during the runs by manual injector compression. The pure water flux ($J_w$) was calculated according to Eq. (4).

$$J_w = \frac{V}{A \cdot t} \quad (4)$$

where $V$ (L) denotes the volume of permeate that is collected during the time interval $t$ (h) and $A$ (m$^2$) is the effective area of membrane.

The rejection efficiency of the membranes was studied by performing filtration of the inorganic salt solutions of $MgSO_4$, $Na_2SO_4$, and NaCl solutions individually at a constant membrane pressure of 0.2 MPa. The feed solutions were prepared at 1 g L$^{-1}$ and pH = 6.0. The pH was regulated by 0.1 M HCl or NaOH addition. The feed and the collected permeate were tested using a conductivity meter. The solute rejection percentage (SR) was then calculated by Eq. (5) shown below.

$$\text{SR}\% = \left[1 - \frac{C_p}{C_f}\right] \times 100 \quad (5)$$

where $C_f$ and $C_p$ are the concentrations of the feed and the permeate, respectively.

### 5.2. Antifouling performance

Sodium alginate (SA) was used in the fouling experiments as a model of an organic foulant. Experiments were carried out using 20 mg L$^{-1}$ SA and 10 mM NaCl solution as follows. First, the SA solution was applied as a feed solution until the flux was almost stable. After that, the flux equipment parts and membranes were washed out with distilled water. After cleaning, the experiments were repeated with distilled water to evaluate the pure water flux and then to determine the flux recovery ratio (FRR) using the following equation. The process also was repeated to examine the membrane stability.

$$\text{FRR}\% = \left(\frac{J_{w2}}{J_{w1}}\right) \times 100 \quad (6)$$

where $J_{w1}$ is the pure water flux before fouling experiment and $J_{w2}$ is the pure water flux after the fouling experiment.

## 6. Results and discussion

### 6.1. Fourier transforms infrared (FT-IR) analysis

Fig. 1 illustrates the FT-IR spectra of the MMT and PVC composites. The MMT spectrum showed peaks at about 3,619 and 1,633 cm$^{-1}$, and they were assigned to the O–H stretching and bending, respectively; the broad peak at 3,449 cm$^{-1}$ was due to the intra-layer hydrogen bonding upon stretching. Moreover, the 1,060 cm$^{-1}$ intensive band was due to Si–O stretching, while the band around 525 cm$^{-1}$ was due to Si–O bending; the peak at 795 cm$^{-1}$ was ascribed to Al–O–Si stretching vibration. In comparison, the infrared spectra obtained for the composites spectra showed the characteristic peaks for the PVC polymer around 2,970 and 2,910 cm$^{-1}$ for the C–H stretching, 1,427 cm$^{-1}$ for $CH_2$ bending, 1,099 cm$^{-1}$ for C–C stretching, and 616 cm$^{-1}$ for C–Cl stretching. In addition to

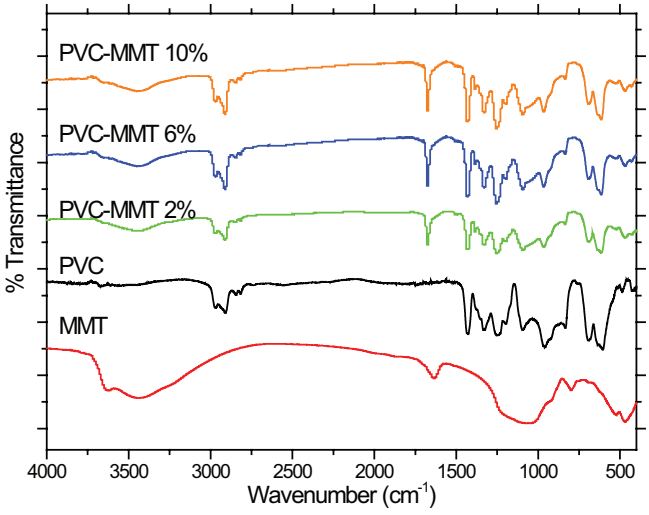


Fig. 1. FT-IR spectra of the MMT and the composite membranes.

the characteristic peaks of the PVC, bands at 3,449 $cm^{-1}$ and around 1,633 $cm^{-1}$ also appeared in the composites spectra and correspond to the MMT. However, the MMT bands at 795 and 1,060 $cm^{-1}$ disappeared in the PVC composites, reflecting possible exfoliation and/or intercalation reactions of the polymer within the clay layers. This disappearance refers to the participation of the Si–O in the interaction. Also, the peak at 1,633 $cm^{-1}$, assigned for OH deformation, was sharper and shifted to higher intensity at 1,681 $cm^{-1}$ [35].

### 6.2. XRD analysis study

The XRD diffractograms of the MMT and the composite membranes are shown in Fig. 2. In Fig. 2, the MMT showed a dominant peak at 2θ = 26.6° corresponding to a basal spacing of 3.35 A°. In contrast, the PVC composites revealed an amorphous morphology. The original characteristic MMT peaks disappeared in the composites diffractograms after the interaction between the polymer and clay. This could be an indication of the possible exfoliated structure formation and the expanded layer distance of the MMT [36]. It is reported that if the peaks of clay appeared in the composite pattern, it reflects a physical mixing between clay and polymer without interaction [37]. As the polymer intercalated within the clay interlayer, the characteristic peaks of MMT clearly disappeared. This finding explains the intercalation of the polymeric network into the stacked silicate galleries of the clay and/or the exfoliation of the clay within the polymer matrices.

This explanation can also be supported by the FTIR results. The formation of the exfoliated structure in the polymer composite could be also due to the possible interaction between the hydroxylated group of MMT and the chloride group of the PVC as might be marked by the shift in the O–H bending band at 1,633 $cm^{-1}$, the deformation of the O–H band at 3,619 $cm^{-1}$, and the disappearance of the Al–O–Si band at 795 $cm^{-1}$.

### 6.3. Morphology of the membranes

The morphology of the PVC composite membranes was studied by the SEM analysis and the results are shown in Fig. 3. Differences were observed between the pure PVC surface taken before and after the addition of MMT. The pure PVC had a smoother surface as shown in the SEM images. Furthermore, the smoothness of the surface was found to decrease with the MMT addition. The structure of the composite membranes appeared porous, and it showed clear differences in the density of the pores when compared with the pure PVC membrane. The observed porous structure could be explained by the solvent water exchange process that occured through the phase-inversion preparation procedure. Moreover, the greater affinity of the MMT particles towards water gives credence to this possibility [38]. This may also cause the formation of the macrovoids, resulting in greater pore size, supported by the trend obtained by increasing the MMT to 10%; this 10% MMT addition led to a convergence of the pores and an increase in the diameter of the pore size. However, as it is known that an increase of the MMT content increases the viscosity of the casting solution, this could also inhibit the water solvent exchange through the phase-inversion process and, consequently, may change the surface structure and affect the pore size. Furthermore, the appearance of MMT particles of various sizes in the SEM micrograph may be due to possible aggregation and poor dispersal when compared with different ratios of MMT content.

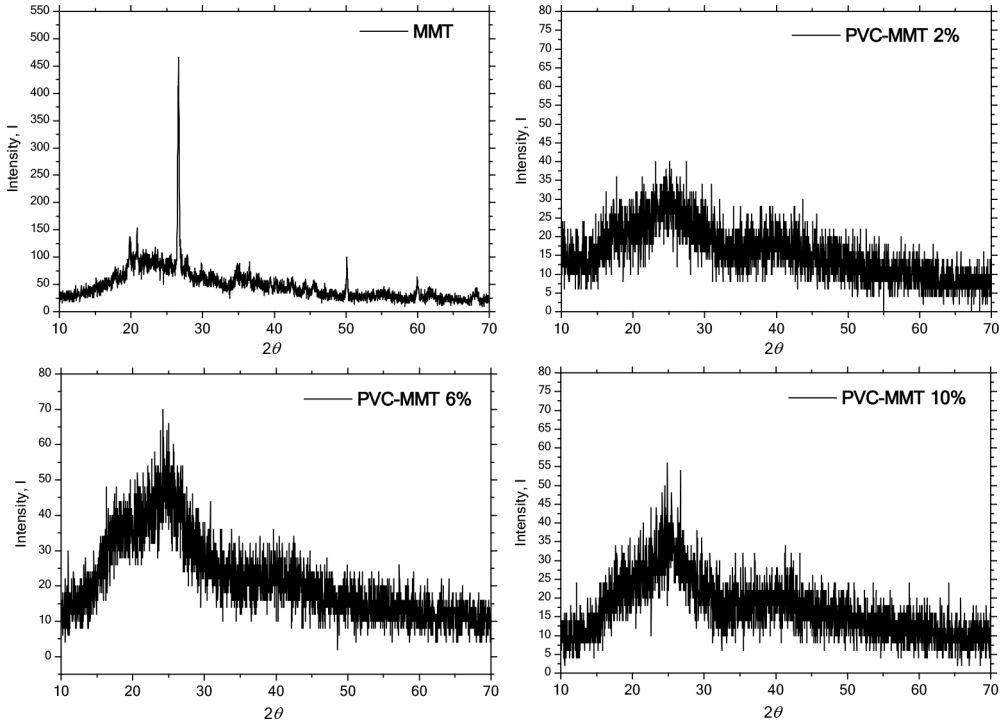


Fig. 2. XRD of the MMT and the composite membranes (PVC-MMT 2% , PVC-MMT 6% and PVC-MMT 10%) as depicted.

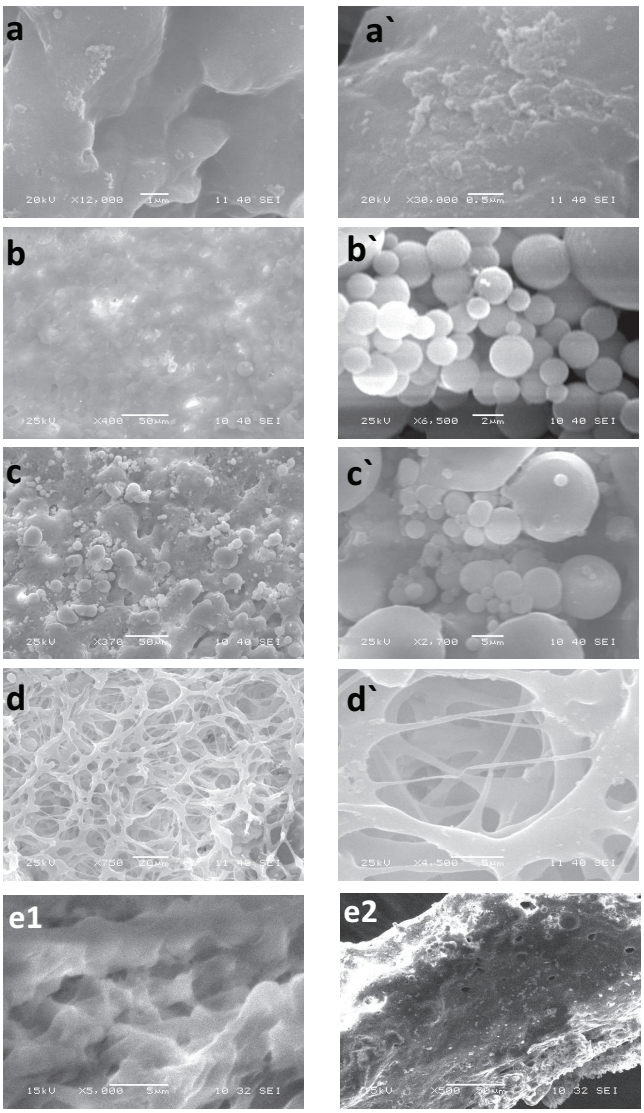


Fig. 3. FESEM surface images of the PVC and the PVC-MMT % composite membranes: (a) pure PVC, (b) PVC-MMT 2%, (c) PVC-MMT 6%, (d) PVC-MMT 10%. (e1) cross sectional PVC, (e2) cross sectional for PVC-MMT 6%.

The cross-section morphology of the membranes given in the SEM images refers to the presence of extended pores within the membrane thickness.

### 6.4. Properties of the membranes

The effects of the MMT content on the properties of the composite membrane in terms of porosity and pore size, as determined by the volume fraction approach, are listed in Table 2. Both porosity and mean pore size were increased with MMT and had a maximum value when the MMT content was 2%. Additionally, Fig. 4 displays the water uptake measurement values of the PVC and composite membranes with different MMT concentrations. The water uptake was found to increase with the addition of MMT; the highest water value uptake reached was 23% with the 10% MMT composite membrane.

### 6.5. Contact angles measurements

As seen in Fig. 5, the contact angle of the pure PVC membrane was 77°, which is consistent with the literature [29]. When MMT was added, the 2% and 6% addition of MMT enhanced the hydrophilicity (i.e., resulted in lower contact angles). This is due to the hydrophilic nature of MMT. Conversely, with the addition of 10% MMT, the membrane

Table 2
Properties of the PVC-MMT% composite membranes

| MMT content (wt%) | Porosity (%) | Thickness (mm) | Mean pore diameter (nm) |
|---|---|---|---|
| 0 | 71.16 | 0.3 | 17.44 |
| 2 | 81.22 | 0.3 | 32.61 |
| 6 | 78.11 | 0.3 | 30.22 |
| 10 | 77.19 | 0.3 | 29.12 |

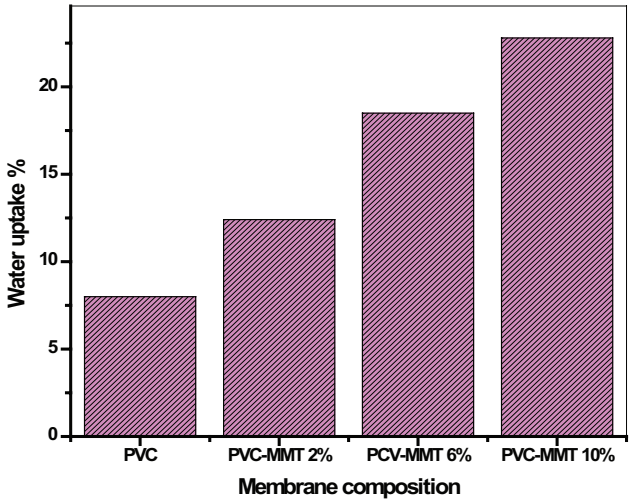


Fig. 4. Water uptake values of PVC-MMT % composite membrane as indicated.

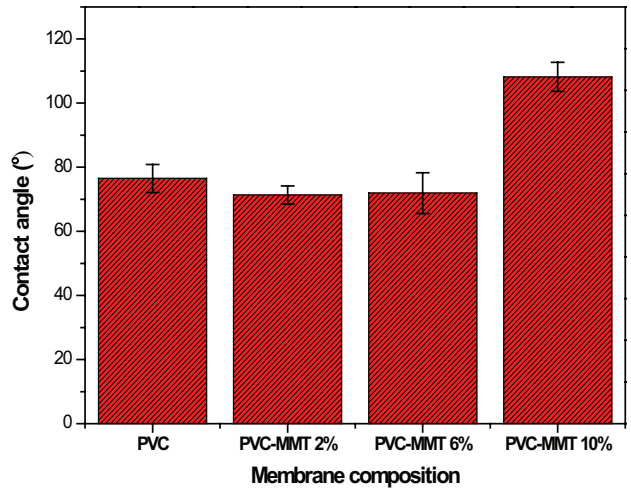


Fig. 5. Static water contact angle of PVC and composite membranes with different MMT concentrations.

exhibited more hydrophobic characteristics. This might be due to the migration of the MMT into the membrane body rather than the membrane surface as seen in the SEM results. This is also in line with the demonstrated water uptake results (Fig. 4). As water uptake increases with the addition of more MMT, this can be an indication of the hydrophilic sub-surface bulk of the PVC-MMT membranes, as a result of the incorporation of the MMT within the polymer structure.

### 6.6. Thermal gravimetric analysis

Based on the observation of the mass loss data at all temperature intervals in TGA curves (Fig. 6), different degradation peaks were observed. One degradation peak was observed for the pure PVC, whereas four degradation peaks were observed for the 2% and 10% MMT composites. The principle degradation step was delayed due to the presence of MMT; this step started at 221°C for the pure PVC and after 249°C for the composite membranes. For the 2%, 6% and 10% MMT composite membranes, the largest decomposition was observed between 256°C–486°C, 252°C–426°C and 249°C–452°C, respectively. For the pure PVC, an interval between 221°C–734°C was observed. If we consider the decomposition temperature at about 50% weight loss, the results clearly indicate higher thermal decomposition temperatures with the composite membranes. Accordingly, the MMT-loaded membranes clearly demonstrate better thermal stability than the pristine PVC.

### 6.7. Membrane performance

The experimental results for performance included pure water flux, solutes rejection, antifouling, and water uptake of the different prepared composite membranes. As illustrated in Fig. 7, the pure water flux increased with pressure as well as with the presence of MMT to reach a maximum of about 1863 L/m$^2$ h with the 10% MMT composite membrane at a pressure of 0.9 MPa. Likewise, in the case of a 6% MMT composite membrane, a pure water flux value of 352 L/m$^2$ h was obtained at 0.2 MPa, compared with 123 L/m$^2$ h with the pure PVC. This means that the composite membranes exhibited a noticeable improvement with the addition of MMT. In fact, the obtained pure water flux was similar when compared with other research carried out with PVC/ZnO and low when compared with PVC/$Fe_2O_3$ nanoparticles obtained at the same pressure; the highest pure water fluxes of PVC/ZnO and

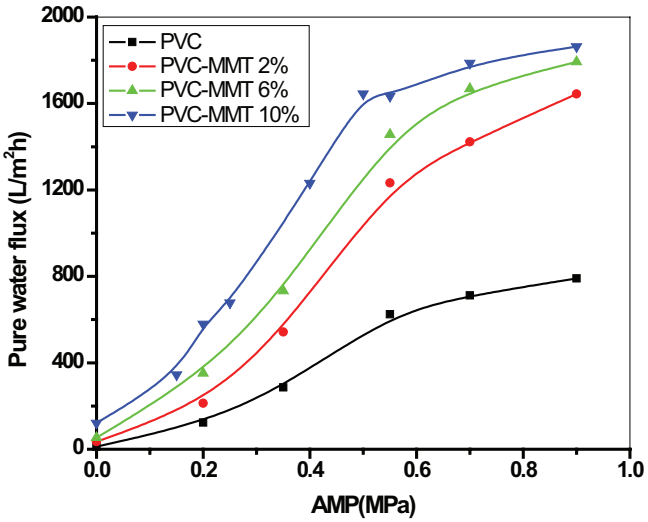


Fig. 7. Pure water flux of the membranes under different MMT-loading concentrations and applied pressure.

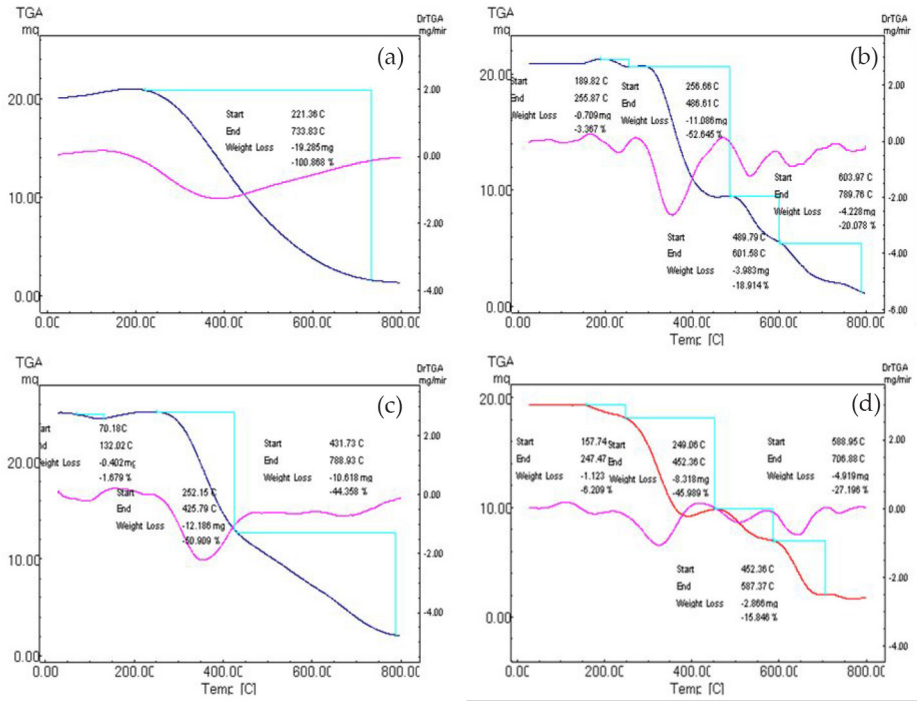


Fig. 6. TGA curves of (a) pure PVC, (b) PVC-MMT 2%, (c) PVC-MMT 6%, (d) PVC-MMT 10% composite membranes.

PVC/$Fe_2O_3$ were 402 L/m² h [14] and 1181 L/m² h [30] respectively at 0.2 MPa. The obtained enhanced water flux for PVC-MMT composite membranes could be explained mainly by the increase of the permeability of the composite membrane, and partially by the increase of the surface hydrophilicity. The addition MMT significantly increased permeability compared with the pristine PVC. The increase of the permeability was due to the increase of the porosity and the mean pore size as a result of the addition of MMT (see Table 2). This was also supported by the SEM results. Moreover, interlayer expansion of MMT may also affected the porous structure, enhancing permeability. Besides the impact on porosity, MMT affinity towards water molecules might have made the composite membranes more favorable to increased water flux. This can be supported by the highest water flux and water uptake value with the 10% MMT composite membrane despite its lower surface hydrophilicity (Fig. 4).

Fig. 7 also shows the effect of the applied pressure on the pure water flux measurements, indicating the stability of the membrane [39]. As shown in Fig. 7, the water fluxes of all membranes were linear, with a pressure change up to about 0.55 MPa and exhibiting resistance to deformation. After that, the flux values started to stabilize to some extent due to the pore deformation. However, composite membranes appeared to be less susceptible to compaction with pressure above 0.55 MPa, particularly for the 2% and 6% MMT loaded membranes, compared with the pure PVC. Similar findings were reported for PVDF/$TiO_2$ composite membranes [40].

Regarding solutes rejection, all the composite membranes exhibited considerable rejection levels from 80% up to 90%, varying with solute types (Fig. 8). Also, a similar solutes rejection pattern was observed for the different composites, with the exception of the 10% MMT. When MMT loading reached 10%, $MgSO_4$ demonstrated higher rejection compared with the NaCl. Moreover, although an increase in pore diameter was observed with the addition of MMT (Table 2), this study revealed up to a 36% improvement in the solutes removal, indicating possible influence of other factors. For example, with the 6% MMT composite membrane, the rejection percentage values obtained for the NaCl and $Na_2SO_4$ increased from about 68% to 87% and 90%, respectively. In contrast, $MgSO_4$ and LiCl demonstrated an increase from about 62% and 59% of the rejection percentage to 82% and 80%, respectively. The observed selectivity enhancement could be an indication of the influence of possible factors such as ion exchange and surface charges. Indeed, the obtained results clearly demonstrate enhanced membrane performance for both permeability and solute rejection, contrasting with the well-known trade-off relationship between permeability and selectivity.

To investigate the impact of the additive content on the antifouling feature of the membranes, the flux recovery ratio (FRR) analysis was performed for the prepared membranes. According to Fig. 9, the pure PVC membrane demonstrated a 73% FRR value. The addition of the MMT led to an apparent improvement in antifouling properties, resulting in higher FRR values. In particular, the 6% MMT composite membrane showed the highest FRR of 91%, representing a 28% improvement compared with the pure PVC. In comparison, although the membrane of 2% MMT also showed an improved fouling behavior, it has a lower FRR value compared with the 6% MMT composite. This could be explained by its larger pore diameter (see Table 2). As the main mechanism of membrane fouling is the adsorption of foulants on the surface and entrapment within the pores, the larger pores of 2% MMT composite could be the reason for its decreased ability for recovery. Generally, the improvement of the FRR could be mainly attributed to the hydrophilic spots of the composite membranes, which inhibited the foulant and the membrane surface's hydrophobic interaction. The fouling reversibility originates from the weak bonding between the foulant and the membrane material, so they were easily washed out of the membrane. This is consistent with what has been reported in the literature: the membrane hydrophilicity is the controlling parameter in the adsorption properties [41]. More hydrophilic content should decrease surface

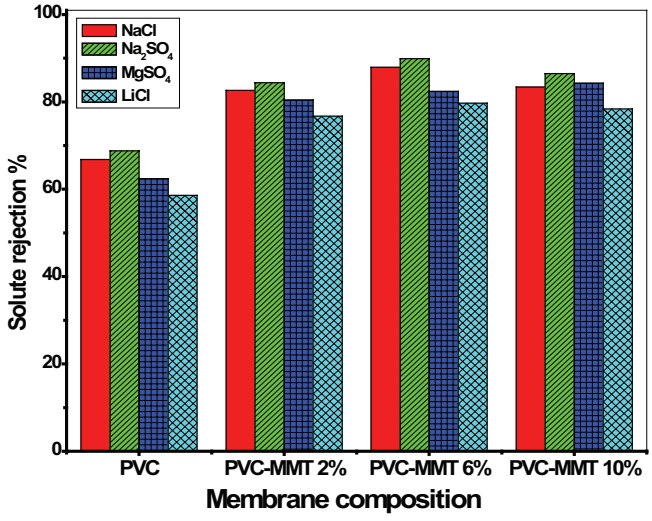


Fig. 8. Solutes rejection of PVC-MMT% composite membranes as indicated.

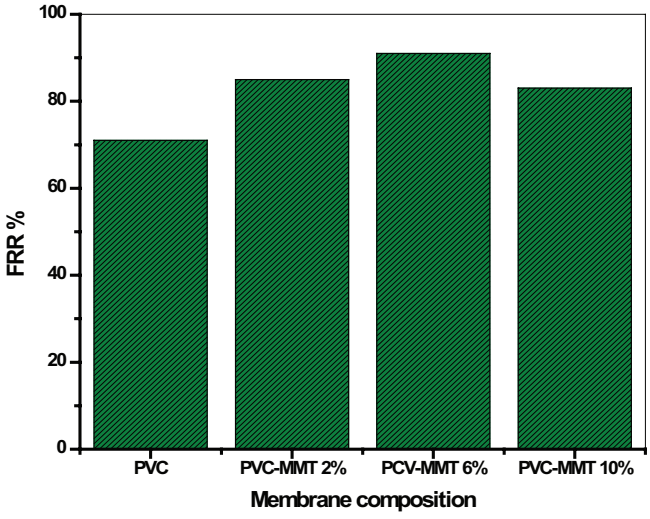


Fig. 9. Water flux recovery ratio of PVC-MMT% membranes after SA fouling.

Table 3
Water flux recovery ratio of PVC-MMT% membranes after repeated SA fouling-cleaning cycles

| Cleaning cycles | PVC | PVC-MMT 2% | PVC-MMT 6% | PVC-MMT 10% |
|---|---|---|---|---|
| FRR% after 1st fouling-cleaning | 73 | 85 | 91 | 83 |
| FRR% after 2nd fouling-cleaning | 71 | 85 | 91 | 83 |
| FRR% after 3rd fouling-cleaning | 67 | 81 | 88 | 78 |
| FRR% after 4th fouling-cleaning | 65 | 78 | 87 | 76 |

fouling as the sorption of hydrophobic agent decreases [18]. Consequently, the addition of MMT greatly enhances the membrane's hydrophilicity and improves the antifouling behavior. These results were also consistent with the contact angle measurements. This is also supported by the FRR value decrease with further addition of MMT (PVC-MMT 10%), which could be related to the decrease in the surface hydrophilicity with the addition of 10% MMT. Nevertheless, the 10% MMT composite membrane, even having lower hydrophilicity than the pure PVC, exhibited a higher FRR value than the pure PVC. This could shed light on the effect of MMT even when it is distributed inside the body or through pores. Accordingly, this would suggest that SA fouling on the membrane surface was more reversible as a result of the higher hydrophilicity owing to the presence of MMT.

It is well known that as the membrane flux increases, the probability of fouling likewise increases [42]. This could be the cause of the lower FRR value for the 10% MMT composite. Although, the presence of hydrophilic MMT in the composite membrane improves the interfacial resistance of the membrane, the accumulation of inorganic particles may increase the fouling as it increases the penetration/adhesion of the foulants at high content ratio of MMT.

Moreover, the results in Table 3 show the pure water flux recovery of the membranes after repeated SA fouling-cleaning cycles. The results clearly show that the membranes are relatively stable until the fourth cycle. These findings regarding stability and enhanced FRR performance demonstrate the potential application of the MMT-loaded composite membrane for water treatment.

## 7. Conclusions

The presence of MMT was found to result in improved performance of the PVC membrane. In particular, composite membranes with 6% MMT was found to result in an optimum performance regarding solutes rejection efficiency and antifouling properties, in addition to enhanced thermal stability and improved water flux. The water flux was found to increase up to 127% with MMT, and at the same time, all membranes showed enhanced removal of NaCl, $Na_2SO_4$, $MgSO_4$ and LiCl up to 87%, 90%, 82%, and 80%, respectively.

## Acknowledgements

The authors acknowledge King Abdul-Aziz City for Science and Technology (KACST) for funding this work through grant number (1-17-01-010-0004).

## Symbols

| | | |
|---|---|---|
| $\varepsilon$ | – | Membrane porosity |
| $J_w$ | – | Pure water flux |
| $Q_w$ | – | Pure water flux |
| $\rho_w$ | – | Density of water |
| $A$ | – | Filtration area |
| $C_f$ | – | Concentration of the feed |
| $C_p$ | – | Concentration of the permeate |
| $J_{w1}$ | – | Pure water flux before foluing |
| $J_{w2}$ | – | Pure water flux after fouling |
| $t$ | – | Time interval |
| $W_d$ | – | Weight for dry membrane |
| $W_w$ | – | Weight for wet membrane |
| $\Delta P$ | – | Transmembrane pressure |
| FRR% | – | Flux recovery ratio |
| SR% | – | Solute rejection percentage |
| $V$ | – | Volume of permeate |
| $a$ | – | Mean pore diameter |
| $l$ | – | Thickness of membrane |
| $r$ | – | Radius of membrane |
| $\mu$ | – | Viscosity of water |

## References

[1] C. Chen, L. Tang, B. Liu, X. Zhang, J. Crittenden, K.L. Chen, Y. Chen, Forming mechanism study of unique pillar-like and defect-free PVDF ultrafiltration membranes with high flux, J. Membr. Sci., 487 (2015) 1–11.
[2] Q. Yang, Z.K. Xu, Z.W. Dai, J.L. Wang, M. Ulbricht, Surface modification of polypropylene microporous membranes with a novel glycopolymer, Chem. Mater., 17 (2005) 3050–3058.
[3] H. Susanto, M. Ulbricht, Characteristics, performance and stability of polyethersulfone ultrafiltration membranes prepared by phase separation method using different macromolecular additives, J. Membr. Sci., 327 (2009) 125–135.
[4] N. Scharnagl, H. Buschatz, Polyacrylonitrile (PAN) membranes for ultra- and microfiltration, Desalination, 139 (2001) 191–198.
[5] E. Saljoughi, T. Mohammadi, Cellulose acetate (CA)/polyvinylpyrrolidone (PVP) blend asymmetric membranes: preparation, morphology and performance, Desalination, 249 (2009) 850–854.
[6] R.W. Baker, Overview of Membrane Science and Technology, in: Membrane Technology and Applications, (2004), pp. 1–23.
[7] C. Güell, R.H. Davis, Membrane fouling during microfiltration of protein mixtures, J. Membr. Sci., 119 (1996) 269–284.
[8] A. Akthakul, R.F. Salinaro, A.M. Mayes, Antifouling polymer membranes with subnanometer size selectivity, Macromolecules, 37 (2004) 7663–7668.
[9] P. Wang, K.L. Tan, E.T. Kang, K.G. Neoh, Antifouling poly(vinylidene fluoride) microporous membranes prepared via plasma-induced surface grafting of poly(ethylene glycol), J. Adhes. Sci. Technol., 16 (2002) 111–127.
[10] F. Liu, C.H. Du, B.K. Zhu, Y.Y. Xu, Surface immobilization of polymer brushes onto porous poly(vinylidene fluoride)

membrane by electron beam to improve the hydrophilicity and fouling resistance, Polymer, 48 (2007) 2910–2918.
[11] S.J. Oh, N. Kim, Y.T. Lee, Preparation and characterization of PVDF/$TiO_2$ organic–inorganic composite membranes for fouling resistance improvement, J. Membr. Sci., 345 (2009) 13–20.
[12] J.-F. Li, Z.-L. Xu, H. Yang, L.-Y. Yu, M. Liu, Effect of $TiO_2$ nanoparticles on the surface morphology and performance of microporous PES membrane, Appl. Surf. Sci., 255 (2009) 4725–4732.
[13] L. Shen, X. Bian, X. Lu, L. Shi, Z. Liu, L. Chen, Z. Hou, K. Fan, Preparation and characterization of ZnO/polyethersulfone (PES) hybrid membranes, Desalination, 293 (2012) 21–29.
[14] H. Rabiee, V. Vatanpour, M.H.D.A. Farahani, H. Zarrabi, Improvement in flux and antifouling properties of PVC ultrafiltration membranes by incorporation of zinc oxide (ZnO) nanoparticles, Sep. Purif. Technol., 156 (2015) 299–310.
[15] N. Maximous, G. Nakhla, W. Wan, K. Wong, Preparation, characterization and performance of $Al_2O_3$/PES membrane for wastewater filtration, J. Membr. Sci., 341 (2009) 67–75.
[16] X. Liu, Y. Peng, S. Ji, A new method to prepare organic-inorganic hybrid membranes, Desalination, 221 (2008) 376–382.
[17] J. Zhang, Z. Xu, M. Shan, B. Zhou, Y. Li, B. Li, J. Niu, X. Qian, Synergetic effects of oxidized carbon nanotubes and graphene oxide on fouling control and anti-fouling mechanism of polyvinylidene fluoride ultrafiltration membranes, J. Membr. Sci., 448 (2013) 81–92.
[18] V. Vatanpour, S.S. Madaeni, R. Moradian, S. Zinadini, B. Astinchap, Novel antibifouling nanofiltration polyethersulfone membrane fabricated from embedding $TiO_2$ coated multiwalled carbon nanotubes, Sep. Purif. Technol., 90 (2012) 69–82.
[19] V. Vatanpour, M. Esmaeili, M.H.D.A. Farahani, Fouling reduction and retention increment of polyethersulfone nanofiltration membranes embedded by amine-functionalized multi-walled carbon nanotubes, J. Membr. Sci., 466 (2014) 70–81.
[20] G. Wu, S. Gan, L. Cui, Y. Xu, Preparation and characterization of PES/$TiO_2$ composite membranes, Appl. Surf. Sci., 254 (2008) 7080–7086.
[21] V. Vatanpour, S.S. Madaeni, A.R. Khataee, E. Salehi, S. Zinadini, H.A. Monfared, $TiO_2$ embedded mixed matrix PES nanocomposite membranes: influence of different sizes and types of nanoparticles on antifouling and performance, Desalination, 292 (2012) 19–29.
[22] X. Cao, J. Ma, X. Shi, Z. Ren, Effect of $TiO_2$ nanoparticle size on the performance of PVDF membrane, Appl. Surf. Sci., 253 (2006) 2003–2010.
[23] J.-n. Shen, H.-m. Ruan, L.-g. Wu, C.-j. Gao, Preparation and characterization of PES–$SiO_2$ organic–inorganic composite ultrafiltration membrane for raw water pretreatment, Chem. Eng. J., 168 (2011) 1272–1278.
[24] J. Liu, Y. Su, J. Peng, X. Zhao, Y. Zhang, Y. Dong, Z. Jiang, Preparation and performance of antifouling PVC/CPVC blend ultrafiltration membranes, Ind. Eng. Chem. Res., 51 (2012) 8308–8314.
[25] Q.F. An, J.W. Qian, H.B. Sun, L.N. Wang, L. Zhang, H.L. Chen, Compatibility of PVC/EVA blends and the pervaporation of their blend membranes for benzene/cyclohexane mixtures, J. Membr. Sci., 222 (2003) 113–122.
[26] M. Bodzek, K. Konieczny, The influence of molecular mass of poly (vinyl chloride) on the structure and transport characteristics of ultrafiltration membranes, J. Membr. Sci., 61 (1991) 131–156.
[27] B. Liu, C. Chen, W. Zhang, J. Crittenden, Y. Chen, Low-cost antifouling PVC ultrafiltration membrane fabrication with Pluronic F 127: effect of additives on properties and performance, Desalination, 307 (2012) 26–33.
[28] J. Xu, Z.-L. Xu, Poly(vinyl chloride) (PVC) hollow fiber ultrafiltration membranes prepared from PVC/additives/solvent, J. Membr. Sci., 208 (2002) 203–212.
[29] Y. Peng, Y. Sui, Compatibility research on PVC/PVB blended membranes, Desalination, 196 (2006) 13–21.
[30] E. Demirel, B. Zhang, M. Papakyriakou, S. Xia, Y. Chen, $Fe_2O_3$ nanocomposite PVC membrane with enhanced properties and separation performance, J. Membr. Sci., 529 (2017) 170–184.
[31] F. Gong, M. Feng, C. Zhao, S. Zhang, M. Yang, Thermal properties of poly(vinyl chloride)/montmorillonite nanocomposites, Polym. Degrad. Stab., 84 (2004) 289–294.
[32] C. Wan, X. Qiao, Y. Zhang, Effect of different clay treatment on morphology and mechanical properties of PVC-clay nanocomposites, Polym. Test., 22 (2003) 453–461.
[33] D. Wang, D. Parlow, Q. Yao, C.A. Wilkie, PVC-clay nanocomposites: preparation, thermal and mechanical properties, J Vinyl Add. Tech, 7 (2001) 203–213.
[34] B. Deng, M. Yu, X. Yang, B. Zhang, L. Li, L. Xie, J. Li, X. Lu, Antifouling microfiltration membranes prepared from acrylic acid or methacrylic acid grafted poly(vinylidene fluoride) powder synthesized via pre-irradiation induced graft polymerization, J. Membr. Sci., 350 (2010) 252–258.
[35] D. Katti, K. Katti, M. Raviprasad, C. Gu, Role of Polymer Interactions with Clays and Modifiers on Nanomechanical Properties and Crystallinity in Polymer Clay, Nanocomposites, 2012.
[36] S. Sarkar, S. Datta, D. Biswas, Synthesis and Characterization of Nanoclay- Polymer Composites from Soil Clay with Respect to Their Water- Holding Capacities and Nutrient- Release Behavior, 2014.
[37] R. Mukhopadhyay, N. De, Nano clay polymer composite: synthesis, characterization, properties and application in rainfed agriculture, Global J. Bio. Biotechnol, 3 (2014) 133–138.
[38] J. María Arsuaga, A. Sotto, G. del Rosario, A. Martínez, S. Molina, S.B. Teli, J. de Abajo, Influence of the type, size, and distribution of metal oxide particles on the properties of nanocomposite ultrafiltration membranes, J. Membr. Sci., 428 (2013) 131–141.
[39] M.T.M. Pendergast, J.M. Nygaard, A.K. Ghosh, E.M.V. Hoek, Using nanocomposite materials technology to understand and control reverse osmosis membrane compaction, Desalination, 261 (2010) 255–263.
[40] K. Ebert, D. Fritsch, J. Koll, C. Tjahjawiguna, Influence of inorganic fillers on the compaction behaviour of porous polymer based membranes, J. Membr. Sci., 233 (2004) 71–78.
[41] B. Khorshidi, J. Hajinasiri, G. Ma, S. Bhattacharjee, M. Sadrzadeh, Thermally resistant and electrically conductive PES/ITO nanocomposite membrane, J. Membr. Sci., 500 (2016) 151–160.
[42] N. Akar, B. Asar, N. Dizge, I. Koyuncu, Investigation of characterization and biofouling properties of PES membrane containing selenium and copper nanoparticles, J. Membr. Sci., 437 (2013) 216–226.